Synthesis and Characterisation of a Lithium Ferrite Electrode for Nuclear Reactor Applications

M. Manley & W. Cook
Department of Chemical Engineering, University of New Brunswick
Fredericton, NB, Canada, E3B 5A3

Abstract

Chemistry control and corrosion measurement have been investigated by researchers in nuclear industry for decades. Electrochemical measurement in extreme conditions has proven difficult, as many electrodes suffer from short lifetimes. Both lithium and ferric oxides are present in nuclear systems, making lithium ferrite an attractive electrode material due to its non-contaminating nature. Lithium ferrite ($LiFe_5O_8$), a spinel-type ferrite, was successfully synthesized and characterized by XRD, SEM and TEM analyses. The determination of identifiable peaks by Laser Raman analysis was achieved and provided a distinction between the ordered (α) and disordered (β) phases. A bulk sample containing more than 50% of the β-phase lithium-ferrite powder could be simply produced through solid state synthesis by combining lithium carbonate and ferric oxide. Electrochemical testing of lithium ferrite pellets in varying concentrations of LiOH solution showed good correlation (92-98%) with Nernstian behavior.

1. Introduction

Experimentation involving lithium ions and the production of lithium compounds has become increasingly popular with the continuing demand for advancement in lithium ion battery technology and the need for variable energy sources. This field of lithium research has lead to developments of new synthesis techniques and new applications of lithium compounds, such as lithium ferrite ($LiFe_5O_8$). (1) Some common uses of lithium ferrite are as a cathode material in rechargeable lithium batteries and as a cheaper alternative to garnet materials in microwave frequency studies. Lithium ferrite is considered as a cathode material due to its environmental benignity, (2) and lithium has a much lower cost compared to other commonly used materials, such as nickel and cobalt. (3) Lithium ferrite, being a spinel ferrite, can be used as a magnetic storage device in applied technology in industry due to its magnetic properties. (4) It may also be possible, due to the potential electrochemical activity of lithium ferrite, for it to be used as an electrode or sensor in a nuclear reactor. Since both ferrous/ferric oxides and lithium (derived from the LiOH used for pH control) are present in a CANDU primary heat transport circuit, a sensor or electrode based on this ferrite would be non-contaminating in the reactor environment and could be a useful tool for measurement of corrosion, electrochemical corrosion potential (ECP) and possibly lithium ion concentration.

Lithium ferrite is a spinel-type ferrite of the type AB_2O_4 with high saturation magnetization and a high Curie temperature. In the ordered α-phase of $LiFe_5O_8$, the Li^+ and Fe^{3+} ions are ordered in a 1:3 molar ratio in the octahedral sites of the cubic spinel. (5) β-$LiFe_5O_8$ has a disordered face centered cubic structure where the Fe^{3+} and Li^+ ions are randomly located in the octahedral interstices.(2)

Lithium ferrite ($LiFe_5O_8$ or $Li_{0.5}Fe_{2.5}O_4$) can exist with an ordered structure or with disorder among the Fe^{3+} and Li^+ ions in the octahedral interstices. The crystal structure of β-$LiFe_5O_8$ has been compared to the inverse spinel structure of magnetite, Fe_3O_4, where half the ferric ions and the lithium ions occupy octahedral interstices, the other half of the ferric ions occupy tetrahedral interstices. (6) A typical spinel structure of the type AB_2O_4 contains a close-packed cubic array of oxygen ions, and only half of the octahedral and one eighth of the tetrahedral spaces are occupied. The unit cell consists of eight molecules. The 32e positions of space group Fd3m are occupied by the oxygen ions. In the AB_2O_4 structure, the B cations occupy the octahedral sites and the A cations occupy the 8a tetrahedral interstices. However, since each 8a tetrahedral site shares a face with four neighboring and empty 16c octahedral sites, there is a diffusion path for the A cations from 8a to 16c. Conversely, the 8b tetrahedral sites share common faces with 16d octahedral sites that are occupied by B cations, making their energy unsuited for cation occupation. Inverse and mixed spinels have the general formula $B[AB]O_4$ and $A_xB_y[A_{1-x}B_{1-y}]O_4$, respectively. Lithium ferrite fits the mixed spinel formula $Fe[Li_{0.5}Fe_{1.5}]O_4$, or $LiFe_5O_8$. (7)

The disordered (β) phase is more likely seen with quenching from high temperatures. Slow cooling provides the condition for the formation of the ordered (α) phase.(2) β-$LiFe_5O_8$ is a good electric conductor and has reproducible conductivity between 22°C-850°C. Its good conductivity is due to its n-type semiconductor properties as well as the considerable mobility of the lithium and ferric ions in the cubic, spinel matrix.(8) $LiFe_5O_8$ possesses both ionic and electric conduction due to the presence of Fe^{3+} and Li^+ ions in the spinel cubic matrix.(8) The α-phase of $LiFe_5O_8$ shows variable conductivity below 740°C when numerous samples are tested. This could be due to the long transition time between α and β phases.(8) The β-phase of $LiFe_5O_8$ desired for the application of this experiment can be produced by the following equation:

$$2Fe_2O_3 + LiFeO_2\ (\alpha \text{ and } \beta) \rightarrow LiFe_5O_8\ (\beta) \tag{1}$$

The above reaction must occur at between 700°C and 1000°C for specifically the β-phase to be produced.(9) Within this temperature range, the lithium ferrite produced has high enough diffusion rates to create a disordered arrangement upon quenching. Above this range, lithium is actually lost and the structure is prone to ordering.

A method of solid state synthesis of lithium ferrite simply involving the reaction between lithium carbonate, Li_2CO_3, and ferrous oxide, Fe_2O_3, has been investigated. At temperatures between 400°C-1000°C, carbon dioxide is evolved and the disordered β–phase of $LiFe_5O_8$ is formed. (10)
The proposed reaction mechanism for the production of $LiFe_5O_8$ is as follows:

$$Li_2CO_3 + Fe_2O_3 \rightarrow 2LiFeO_2 + CO_2 \tag{2}$$

$$LiFeO_2 + 2Fe_2O_3 \rightarrow LiFe_5O_8 \tag{3}$$

This scheme has been proposed after thorough review of thermogravimetric analysis results and XRD. (10) Li_2CO_3 decomposes at temperatures above 400°C, but above 700°C the loss of Li^+ and O^{-2} from the ferrite, combined with a difference in density, allows the combination of $LiFe_5O_8$ into the β-spinel matrix. (9; 10)

2. Experimental

Lithium carbonate powder (Li_2CO_3 from Sigma-Aldrich: CAS 554-13-2, 99+ %) was mixed with fine hematite powder (Fe_2O_3 from Fisher: CAS 1309-37-1, 99+ %) in a 1:5 molar ratio, and the two components were ground with a ceramic mortar and pestle for thirty minutes. The 1:5 molar ratio of lithium carbonate to hematite is necessary to ensure that the second reaction in the mechanism shown in Equation 2 and Equation 3 reaches completion.

Ethanol is added to the powder mixture to ensure homogeneity and is ground with the mortar until all of the ethanol is evaporated. The lithium-carbonate/hematite mixture was placed in three separate ceramic crucibles to compare the effect of cooling rates on the final composition. All three crucibles were heated to 900°C in the Thermo Scientific Thermolyne bench-top furnace at a rate of 33°C/hour to allow slow decomposition of Li_2CO_3. (10) After 3 hours at temperature, the heater was shut off. One crucible was left to slow cool in the furnace for 24 hours, while the other two were removed and quenched in air. To compare quenching rates, the powder from one of the crucibles was poured onto a ceramic plate and broken up to promote increased heat transfer and cooling while the other was left to air-quench in the crucible without being disturbed. The powders were collected in vials and stored.

The electrochemical properties of the three powders were tested in varying concentrations of LiOH solutions from 10^{-4} M to 1 M. The electrode consisted of the fine powder compressed into a pellet around a length of platinum wire. All three electrodes were tested in each concentration of LiOH, where the voltage would be swept at rates of 25, 50, and 100 mV/s between 0.5 V and -0.8 V versus SCE for 3 cycles, measuring the resulting current response from the system. The equilibrium potentials, the potential existing between the oxidation and reduction peak on the resulting cyclic voltammagram, was determined for each trial.

3. Results and Discussion

The powder collected from the quenched samples, expected to include the β-phase of $LiFe_5O_8$, was reddish-brown in appearance and occupied approximately the same volume in the crucible, although it could be seen that some contraction had occurred since the bulk of the sample had rescinded from the crucible walls.

Imaging was completed by scanning electron microscopy (SEM) to view the particles and particle size distribution of the quenched lithium ferrite powder produced through this simple solid-state synthesis route. A JEOL JSM6400 digital SEM with Gellar dPict digital image acquisition software was used. The resulting images, seen in Figures 1(a-b) show the particles are 300 nm or less in diameter, with a fairly even particle size distribution.

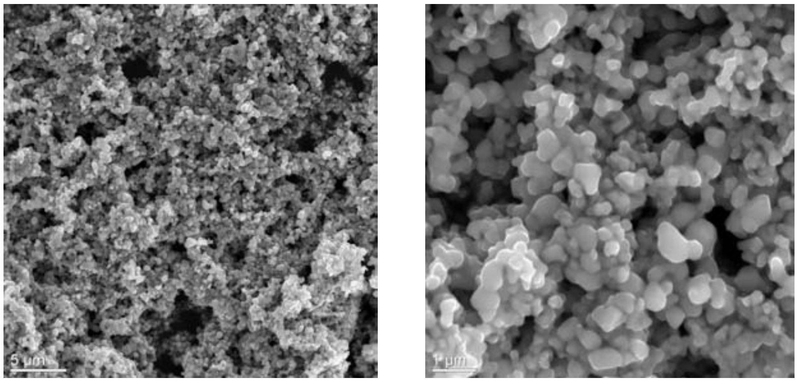

Figures 1(a), left, and 1(b), right: SEM imaging on lithium ferrite powder produced through solid state reaction pathway

The powder was taken and analyzed using X-ray diffraction (XRD) to characterize the products and phases present. The X-ray source was a 2.2 kW Cu X-ray tube with an operating power and current of 40 kW and 30 mA respectively. X-ray optics were the standard Bragg-Brentano para-focusing mode. A step size of 0.02° and 1.0 second were used during the testing. A Pelletier-cooled solid state (Si [Li]) detector (Sol-X) with a useful energy range of 1.60 keV was employed. Raw data was analyzed with the EVA program. XRD results can be seen in Figures 2(a-c).

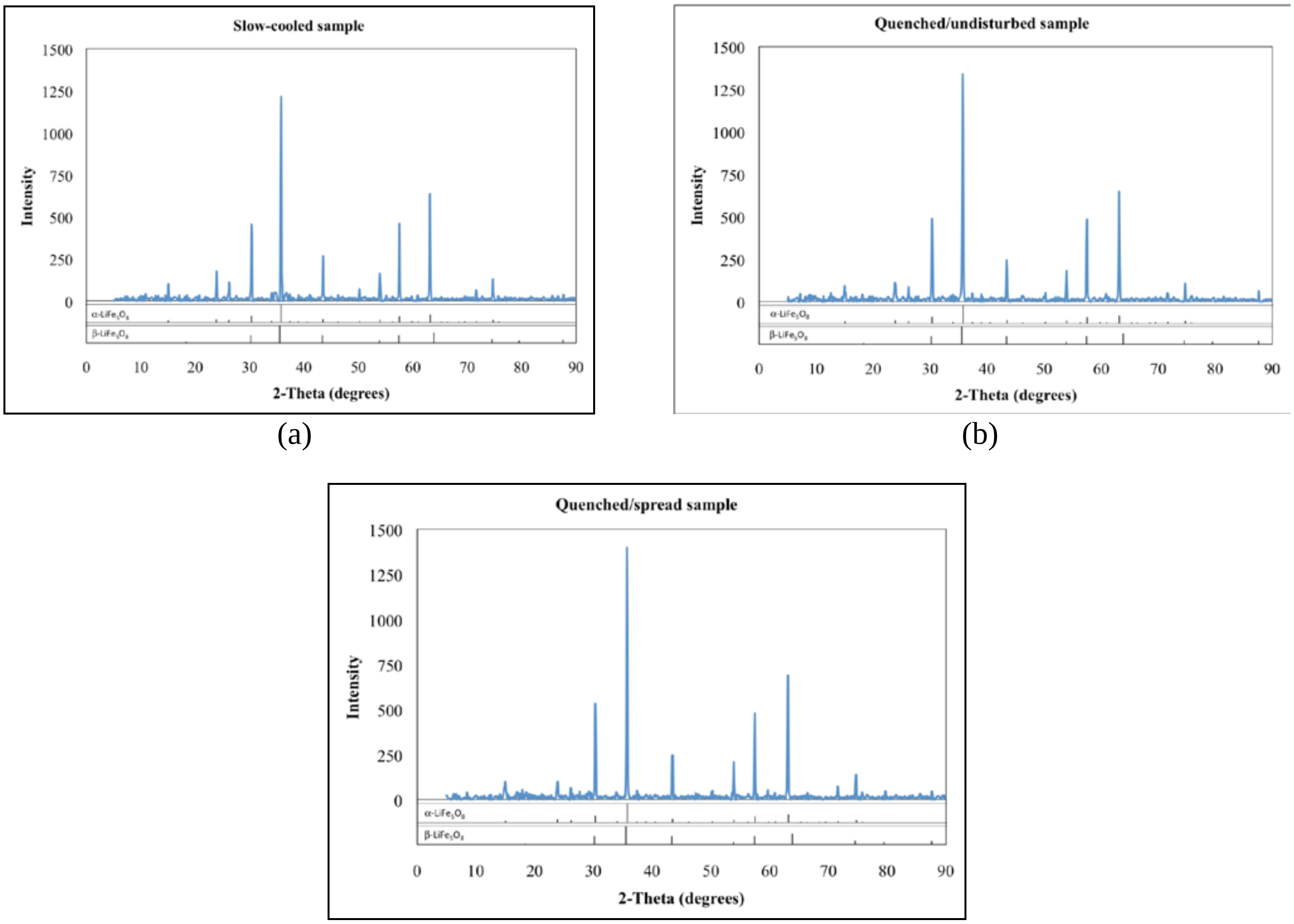

(a)

(b)

(c)

Figure 2(a): XRD data for slow-cooled lithium ferrite powder; (b): XRD data for quenched/undisturbed lithium ferrite powder; (c): XRD data for quenched/spread lithium ferrite powder

The powder was then sent for analysis to retrieve base-line peaks for lithium ferrite (ordered and disordered phases) with a Laser Raman microscope. A Renishaw inVia Raman microscope was employed. The microscope uses a He-Ne gas mixture @ 633nm, considered to be a mid-range wavelength. The base line peaks for the ordered and disordered lithium ferrites from the Raman characterization are shown in Figures 3(a-b), respectively.

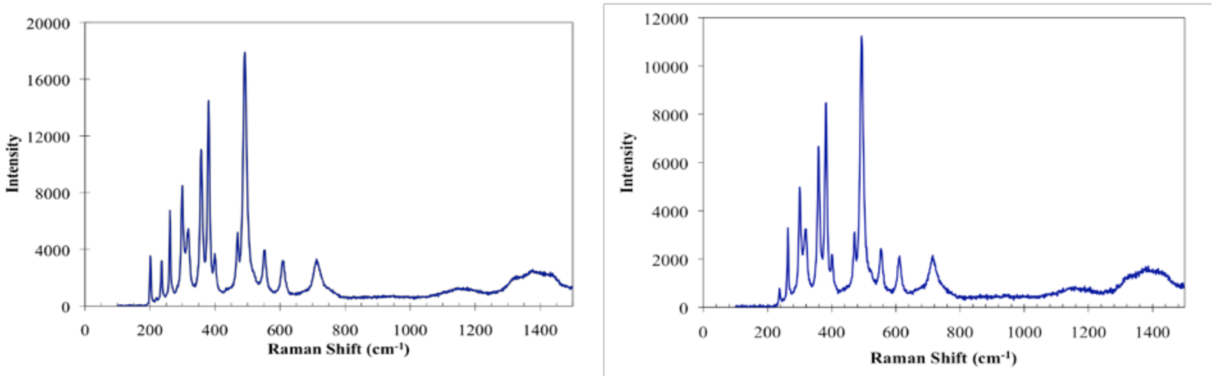

(a) (b)

Figure 3(a): Raman spectra for ordered lithium ferrite; (b): Raman spectra for disordered lithium ferrite

The characteristic peaks of ordered and disordered lithium ferrite for Laser Raman analysis was generated from Figures 3(a-b) and is shown in Table 1.

Table 1: Primary Laser Raman peaks for α- and β-phase lithium-ferrite in decreasing order of intensity.

Peak	1	2	3	4	5	6	7	8	9	10	11	12	13
Raman Shift (cm^{-1})	493	382	358	300	263	318	469	553	400	201*	716	610	236*

*peaks not expected to be present in β-$LiFe_5O_8$

The XRD spectrum, shown in Figures 2(a-c) confirms that that powder produced did indeed contain a significant portion of the disordered β-phase of $LiFe_5O_8$. As there are few distinguishing peaks for the β-phase compared with the α-phase, one must look at the diminishing proportions of two supplementary peaks that are present for the α-phase to confirm the presence of the β-phase in the bulk sample. The slow-cooled powder produced purely α-phase $LiFe_5O_8$, seen in Figure 2a. The peaks at 23.8°, 26.2° (offset by 5 degrees) and 50.5° are clearly diminished in Figure 2b, the XRD graph of the air quenched but undisturbed powder. The lower end peaks are even further diminished for the air quenched and distributed powder - Figure 2c, as the powder is more quickly quenched, preserving more of the disordered phase. By comparing the slow-cooled graph, the quenched/undisturbed graph and the quenched/spread graph, we see the proportions between the peaks at diffractions angles 35.8°, 23.8° and 26.2° decrease from 0.147 and 0.092 in the pure α-phase powder to 0.0889 and 0.0556 in the quenched/undisturbed powder and to 0.072 and 0.045 in the quenched/spread powder. The peak at 35.8° is used as a reference as it is the strongest peak in common with both α and β phases. Assuming the slow-cooled powder is purely α-phase, this corresponds to approximately 38% β-phase formed in the undisturbed powder and between 50-55% β-phase retained in the quenched/spread powder.

Raman characterization of α-phase $LiFe_5O_8$ in Figure 3a clearly exhibits a peaks in the 200-250 cm^{-1} region, one of which at 202 cm^{-1} that is not visible on the Raman scan of the predominately β-phase ferrite in Figure 3b. The other low-end peak, at 236 cm^{-1}, is clearly diminished in the sample containing the β-phase indicating a significantly reduced fraction of α-phase in the sample. The main peaks identifying α- and β-$LiFe_5O_8$ by the Laser Raman analysis are listed in Table 1. Of note is the absence of the peak at 202 cm^{-1} when the β-phase is present and the shrinking intensity of the peak at 236 cm^{-1}. Presumably, in a pure β-$LiFe_5O_8$ sample, both these peaks would vanish.

Diffraction patterns and diffraction angles were determined by transmission electron spectroscopy (TEM) to further confirm the presence of β-$LiFe_5O_8$. The instrumentation employed was a JEOL 2011 STEM with Gatan imaging filter (GIF 2000), Gatan 4k x 4k Ultrascan digital camera, and atomic structure –Z- contrast imaging (HAADF). The JEOL 2011 also used energy filtered TEM (EFTEM). Figure 4 exhibits the diffraction pattern obtained from the air-quenched then spread lithium ferrite sample.

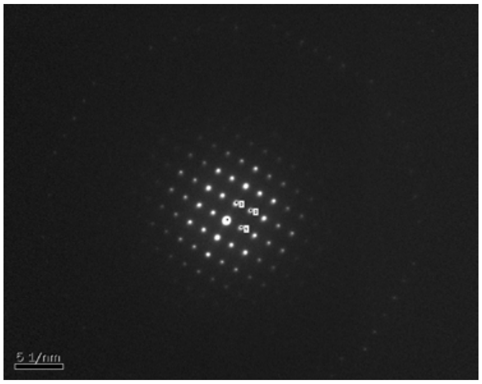

Figure 4: TEM image displaying disorder diffraction angles

TEM diffraction patterns were obtained for the air-quenched then spread powder. The resulting d-spacing measurements showed that there was a degree of disorder within the sample. The longest characteristic d-spacing for β-$LiFe_5O_8$ is 4.84 Å, and it is 5.89 Å for α-$LiFe_5O_8$ according to the JCPDS-ICDD database used for the TEM referencing software. Spots measured on the grain showed d-spacings of 4.88 Å and 5.92 Å; therefore, the sample must contain both ordered and disordered lithium ferrite. A pure sample of α-$LiFe_5O_8$ would not contain any d-spacing in the range of 4.8 Å.

Table 2 shows the symbols used to distinguish the three powders after they were compressed into individual electrodes. The lithium ferrite is expected to follow the redox equation, shown in Equation 4 below, whereby lithium ferrite is reduced to $LiFe_2O_3$ and Fe_3O_4 with the exchange of two electrons. The reactions would be considered completely reversible if the lithiated hematite, $LiFe_2O_3$, were to recombine with the magnetite, Fe_3O_4, to form lithium ferrite.

Table 2: Symbols used to relate corresponding powders and electrodes

Powder	**Electrode Designation**	**% β-phase**
Slow-cooled	α	~0
Quenched - undisturbed	α+β	38
Quenched - spread	β	50-55

$$LiFe_5O_8 + 2e^- + H_2O \Leftrightarrow LiFe_2O_3 + Fe_3O_4 + 2OH^- \qquad (4)$$

For a given system, the Nernst equation can be rewritten to show that with all variables are known except for the experimentally determined equilibrium potential and the pH. A plot of equilibrium potential versus pH should therefore be linear. The results of the experimentally determined equilibrium potential and pH plotted for each of the three electrodes is shown below in Figures 5(a-c).

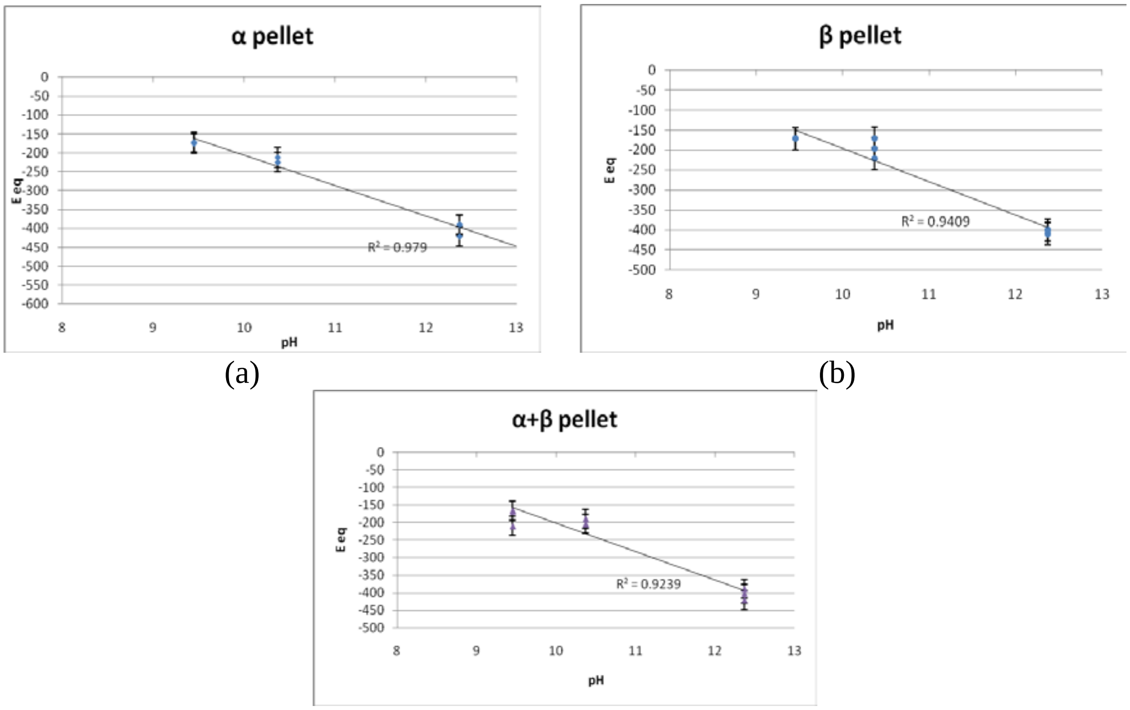

(a) (b)

(c)

Figure 5(a): Nernstian correlation for α pellet at room temperature; (b): Nernstian correlation for α-β pellet at room temperature; (c): Nernstian correlation for β pellet at room temperature

4. Conclusions

The synthesis of lithium ferrite led to the determination of identifiable peaks by Laser Raman analysis and provided a distinction between the ordered (α) and disordered (β) phases. It was found that by combining lithium carbonate powder with fine hematite powder in a 1:5 molar ratio, heating the well-blended mixture in air at 900°C for 3 hours and air quenching to room temperature, a bulk sample containing greater than 50% of the β-phase lithium-ferrite powder could be simply produced. SEM images of the β-$LiFe_5O_8$ powder showed particles less than 300 nm in diameter with an even particle distribution.

The composition of the powder was confirmed by XRD analysis to be pure lithium ferrite ($LiFe_5O_8$) containing a significant amount of the desired β-phase (between 38-55%), the proportion increasing with faster quenching from high temperature. The various forms of the lithium-ferrite powder were analyzed by Laser Raman spectroscopy to provide a reference set of peaks identifying the different lithium-ferrite phases. The largest peaks resulting from the Raman analysis were found to be 493, 382, 358, 300, and 263 (shift, cm^{-1}). The peaks at 202 and 236 cm^{-1} are present for the α-phase powder but disappear when considerable β-phase is present, which provides a clear indicator for the presence of β-$LiFe_5O_8$.

TEM diffraction patterns further confirmed the presence of β-$LiFe_5O_8$. The d-spacing measurement of the air-quenched then spread sample of lithium ferrite contained characteristic d-spacings of both α- and β- $LiFe_5O_8$, represented by 5.92 Å and 4.84 Å respectively.

The E_{eq} versus pH graphs to determine the Nernstian correlations showed excellent results for the α, α+β, and β pellets at room temperature with R^2 values of 0.9790, 0.9239, and 0.9409 respectively. This means that the experimentally determined E_{eq} values closely follow the Nernst equation and that the proposed reaction scheme is sound. This also indicates the likelihood for a reversible reaction between the lithium ferrite and its decomposition products meaning that a reference electrode could potentially be assembled with this material.

5. References

[1] Yong An, S., Shim, I., & Kim, C. S., "Synthesis and magnetic properties of $LiFe_5O_8$ powders by a sol-gel process" Journal of Magnetism and Magnetic Materials, Vol. 290, 2004, pp. 1551.

[2] Wang, S., Gao, L., Li, L., Zheng, H., Zhang, Z., Yu, W., et al., "Low-temperature synthesis of metastable lithium ferrite: Magnetic and electrochemical properties" Nanotechnology, Vol. 16, 2005, pp. 2677.

[3] Tabuchi, M., Ado, K., Sakaebe, H., Masquelier, C., Kageyama, H., & Nakamura, O., "Preparation of $AFeO_2$ (A=Li, Na) by hydrothermal method", Solid State Ionics, Vol. 79, 1995, pp. 220.

[4] Dey, S., Roy, A., Das, D., & Ghose, J. Preparation and characterization of nanocrystalline powders of lithium ferrite by citrate precursor methods. Journal of Magnetism and Magnetic Materials, Vol. 270, 2004, pp. 224.

[5] Verma, S., Karande, J., Patidar, A., & Joy, P. A., "Low-temperature synthesis of nanocrystalline lithium ferrite by an autocombustion method using citric acid and glycerine", Materials Letters, Vol. 59, 2005, pp. 2630.

[6] Bogdanovich, M. P., "Relationship between the compositional ordering of solid solutions based on lithium ferrite and the preference energy of the cations for octahedral sites", Sov. Phys. Solid State, Vol. 32, 1990, pp. 3.

[7] Chen, C. J., & Greenblatt, M., "Lithium insertion compounds of $LiFe_5O_8$, $LiFeMn_3O_8$, $Li_2ZnMn_3O_8$. Journal of Solid State Chemistry", Vol. 64, 1986, pp. 240.

[8] Matsui, T., & Wagner, J. B. J., "Electrical properties of $LiFe_5O_8$", Journal of the Electrochemical Society, Vol. 124, 1977, pp. 1141.

[9] El-Shabaky, G. A., & Ibrahim, A. A., "Solid-solid interactions between ferric oxide and lithium carbonate and the thermal stability of the lithium ferrites produced", Thermica Acta, Vol. 118, 1987, pp. 151.

[10] Pointon, A. J., & Saull, R. C., "Solid-state reactions in $LiFe_5O_8$" Journal of the American Ceramic Society, Vol. 52, 1969, pp.157